

# Complex multiannual cycles of *Mycoplasma pneumoniae*: persistence and the role of stochasticity

Bjarke Frost Nielsen<sup>a,1</sup>, Sang Woo Park<sup>b</sup>, Emily Howerton<sup>c</sup>, Olivia Frost Lorentzen<sup>d</sup>, Mogens H. Jensen<sup>e</sup>, and Bryan T. Grenfell<sup>c</sup>

<sup>a</sup>High Meadows Environmental Institute, Princeton University, Princeton, NJ, USA; <sup>b</sup>Department of Ecology and Evolution, University of Chicago, Chicago, IL, USA; <sup>c</sup>Department of Ecology and Evolutionary Biology, Princeton University, Princeton, NJ, USA; <sup>d</sup>Canal Pointe, Princeton, NJ, USA; <sup>e</sup>Niels Bohr Institute, University of Copenhagen, Blegdamsvej 17, DK-2100 Copenhagen, Denmark

This manuscript was compiled on April 16, 2025

**The epidemiological dynamics of *Mycoplasma pneumoniae* are characterized by complex and poorly understood multiannual cycles, posing challenges for forecasting. Using Bayesian methods to fit a seasonally forced transmission model to long-term surveillance data from Denmark (1958–1995, 2010–2025), we investigate the mechanisms driving recurrent outbreaks of *M. pneumoniae*. The period of the multiannual cycles (predominantly approx. 5 years in Denmark) are explained as a consequence of the interaction of two time-scales in the system, one intrinsic and one extrinsic (seasonal). While it provides an excellent fit to shorter time series (a few decades), we find that the deterministic model eventually settles into an annual cycle, failing to reproduce the observed 4-5-year periodicity long-term. Upon further analysis, the system is found to exhibit transient chaos and thus high sensitivity to stochasticity. We show that environmental (but not purely demographic) stochasticity can sustain the multi-year cycles via stochastic resonance. The disruptive effects of COVID-19 non-pharmaceutical interventions (NPIs) on *M. pneumoniae* circulation constitute a natural experiment on the effects of large perturbations. Consequently, the effects of NPIs are included in the model and medium-term predictions are explored. Our findings highlight the intrinsic sensitivity of *M. pneumoniae* dynamics to perturbations and interventions, underscoring the limitations of deterministic epidemic models for long-term prediction. More generally, our results emphasize the potential role of stochasticity as a driver of complex cycles across endemic and recurring pathogens.**

*Mycoplasma pneumoniae* | Epidemiological dynamics | Dynamical systems | Chaos | Stochasticity

The bacterial pathogen *Mycoplasma pneumoniae* is simultaneously common and unusual. It lacks a cell wall and is among the smallest free-living bacteria (1). The infection it causes has been given names such as (*primary*) *atypical pneumonia* (2), *cold pneumonia* and *walking pneumonia* (3) due to its tendency to cause less severe disease compared with typical bacterial pneumonia. It is a very common respiratory pathogen, especially in children and adolescents, and accounts for 15-20% of all cases of pneumonia (4). Disease courses are typically mild, but severe outcomes do occur. About 5-10% of upper airway infections with *M. pneumoniae* progress to pneumonia, and there are likely many asymptomatic cases (5), suggesting a high degree of under-ascertainment. Extrapulmonary symptoms are increasingly recognized (6, 7) and include complications such as encephalitis and RIME/Stevens-Johnson Syndrome (8, 9), with *M. pneumoniae* being the most common infectious cause of the latter in children (10, 11). As many as 25% of *M. pneumoniae* cases develop some extrapulmonary symptoms (12), most commonly dermatological or

gastrointestinal; sometimes cardiovascular (13) and neurological (14) complications are seen, the latter in as many as 1-10% of those *M. pneumoniae* cases which require hospitalization (12, 15, 16).

From an epidemiological dynamics perspective, a remarkable feature of *M. pneumoniae* are the observed complex outbreak cycles, most often with a 3-7 year period (17–20). In Denmark (2), as well as England and Wales (21), 4-5 year cycles have generally been observed. This is in contrast to some classical, strongly immunizing childhood diseases, such as measles, which tend to exhibit simpler annual or biennial dynamics (22), although there are exceptions to that rule, e.g. rubella (23, 24). Despite being such a common pathogen, the mechanisms behind the complex epidemiological dynamics of *M. pneumoniae* remain poorly understood, complicating prediction and forecasting. In general, predictability is important for timely resource allocation and deployment of relevant screening and diagnostic testing schemes. When the year-to-year incidence exhibits wide variability, planning for outbreaks becomes simultaneously more important, and more difficult. Discerning and understanding patterns in this variability is thus paramount for effective planning, not least for *M. pneumoniae*, where severe outcomes are typically preventable if diagnosed and treated in a timely manner.

Since early 2020, the multiannual cycles of *M. pneumoniae* have been largely disrupted (25, 26). This is an example of the polymicrobial effects of the COVID-19-related non-pharmaceutical interventions (NPIs), observed as a disruption of circulation across many pathogens (27) but perhaps ev-

## Significance

The bacterium *Mycoplasma pneumoniae* causes respiratory illness worldwide and is known for its complex and poorly-understood multi-year outbreak cycles. By fitting a mathematical model to data from Denmark spanning several decades, it is shown that a deterministic model can capture the medium-term dynamics, but not the long-term persistence of the multiannual cycles. Instead, environmental randomness – such as variability in host contact patterns – helps sustain the observed 5-year cycles. The work has practical implications for epidemiological forecasting of *M. pneumoniae* and suggests that noise-induced dynamics may be a fundamental driver of complex cycles in endemic pathogens.

<sup>1</sup>To whom correspondence should be addressed. E-mail: bjarke@princeton.edu

idenced most strikingly by the apparent extinction of the Yamagata strain of influenza B virus (28, 29).

Over three years, *M. pneumoniae* circulation was drastically curtailed in many locations and Denmark is no exception. A similar multi-year delay in *M. pneumoniae* resurgence has recently been reported for Europe and Asia (30) as well as the United States (25, 31). Such large-scale perturbations effectively provide a “natural experiment”, demonstrating how the dynamics of *M. pneumoniae* responds to a prolonged disruption and the associated build-up of susceptible individuals, as well as aiding model parameter estimation.

Here, we use a mathematical model that incorporates seasonality, vital dynamics (births/deaths), immunity loss and the effects of NPIs to study recent (2010–2025) and historical (1958–1995) *M. pneumoniae* incidence data from Denmark. The simple deterministic model is found to capture the observed dynamics well over a few decades but eventually reverts to annual outbreaks, failing to reproduce the prominent multi-annual cycles long-term. We show that the presence of environmental noise can indefinitely sustain the multi-year outbreak patterns. In doing so, we highlight the important role that fluctuations in contact patterns, environmental noise, and demographic processes plays when forecasting pathogens with complex dynamics such as *M. pneumoniae*.

## Lessons from contemporary and historical data

We utilize two different data sets as correlates of *M. pneumoniae* incidence, both from Denmark (Statens Serum Institut, SSI). One has *M. pneumoniae*-positive PCR tests (and the raw number of tests performed) with a weekly reporting frequency and covers the period 2010-2025. This data set forms the primary basis for parameter estimation, since the test data is highly *M. pneumoniae*-specific and temporally well-resolved. Secondly, we use a data set covering the period 1958-1995. Beginning in 1946, patient blood samples collected at hospitals and general practitioners for the diagnosis of Primary Atypical Pneumonia (later identified as *M. pneumoniae*) were sent to SSI to undergo the cold agglutinin (CA) reaction. This reaction, unfortunately, has only low to moderate sensitivity ( $\sim 20 - 80\%$  (2, 32)) and moderate specificity ( $\sim 82 - 92\%$  (2, 32)) for *M. pneumoniae*. However, beginning in 1958, CA-positive samples were also subjected to *M. pneumoniae* Complement Fixation (MpCF), which was found to have higher specificity (33, 34). We thus also treat those tests from the 1958-1995 data set which are *simultaneously* CA- and MpCF-positive as an incidence proxy on which we base (secondary) parameter estimates.

The duration of immunity following *M. pneumoniae* infection is known not to be life-long, but the precise duration is unknown, with estimates ranging from a few years to more than a decade (2, 25, 35). For this reason, we opted for an SIRS (Susceptible-Infected-Recovered-Susceptible) compartmental model which allows previously infected individuals to become susceptible, and thus potentially reinfected. The model includes seasonal modulation of the transmission rate and equal birth/death rates (which are assumed constant within each data fit, for simplicity). The duration of immunity was treated as a parameter to be estimated during fitting to data.

The influence of NPIs are implemented as a slowly-varying multiplicative effect on the transmission rate from March 2020 onward, representing a reduction in overall contact rates, the

magnitude of which is an estimated parameter (see Supplementary Fig. S5).

We estimate a basic reproductive number of  $R_0 = 1.8$  (95%CI [1.7, 2.0], in good agreement with ref. (36)), a mean duration of immunity of 11 years and a relative amplitude of seasonality in transmission of 0.19. All estimated parameters and their uncertainties can be found in Table 1.

With a sinusoidal seasonality function\*, the model fits the 2010-2025 data well (with the partial exception of the 2017 season in which the apparent incidence was somewhat higher than modeled), see Fig. 1A. The historical 1958-1995 data, which is overall of much lower fidelity, is captured more loosely by the model, see Fig. 1B. Interestingly, here we had to allow for a slow change in the mean transmission rate and ascertainment (allowed to change only slightly every 4 years), otherwise the model would tend to settle into an annual pattern.

This leads us to a more general observation: the SIRS model with *M. pneumoniae* parameters is able to capture the patterns reasonably well over a few decades, but in the absence of perturbations, the modeled dynamics always decays into an annual pattern eventually. This is of course at odds with the ubiquity of complex multiannual cycles in *M. pneumoniae* (2, 17–21) and other SIRS-like epidemiological systems such as parvovirus B19 (37–41). In the next section we discuss how the time-scales of the *M. pneumoniae* system may give rise to an approximately 5-year cycle, at least transiently. We then go on to investigate the role that stochasticity plays in sustaining such cycles over decades and in re-igniting them even after periods of approximately annual dynamics. In the final part of the paper, we study projections of future *M. pneumoniae* incidence with and without stochasticity.

**Two time-scales conspire to create complex cycles.** The seasonally forced SIRS system with vital dynamics contains two comparable oscillatory time-scales: the one-year seasonal period and the time-scale set by the intrinsic epidemiological dynamics. To ascertain the latter time-scale, the corresponding autonomous system may be studied (that is, the SIRS system with vital dynamics but no seasonal forcing). This system will eventually reach an endemic equilibrium, but will oscillate as it approaches this equilibrium. A linearization of the autonomous system around its endemic equilibrium yields an intrinsic oscillation frequency as well as an exponential decay rate (42), given by a combination of the transmission rate  $\beta$ , immune waning rate  $\delta$ , recovery rate  $\gamma$  and birth/death rate  $\mu$ . Using the parameter values estimated from the Bayesian fit to Danish data (2010-2025), the frequency is found to be  $f_1 = 1/(43.46\text{wk})$  (95%CI: [1/44.0, 1/43.0]). This natural oscillatory time-scale offers a clue to how the 4-5-year cycles come about: denoting the seasonal frequency by  $f_0 = 1/\text{yr}$  and the intrinsic frequency by  $f_1$  as above, the combined effect of the two time-scales can be qualitatively understood by considering the product of two sinusoidal signals with different frequency:

$$\sin(f_0 t) \sin(f_1 t) = \frac{1}{2} (\cos((f_0 - f_1)t) + \cos((f_0 + f_1)t))$$

the resulting signal thus contains a time-scale which is slower than either of the two component time-scales. In our case,

\*We opted for a sinusoidal seasonality function for simplicity, but have also directly estimated the shape of the seasonality function from the data. The resulting seasonality function can be found in Supplementary Fig. S4.

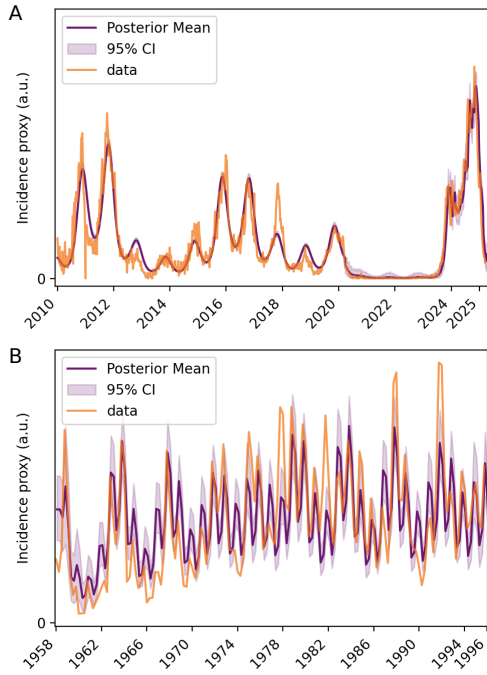


**Fig. 1. Model fits to *Mycoplasma pneumoniae* incidence data.** A seasonal SIRS model is fitted to recent (2010-2025) and historical (1958-1995) *M. pneumoniae* testing data from Denmark using Bayesian inference. **A)** The seasonal SIRS model explains observed *M. pneumoniae* dynamics 2010-2025 well. The fitted data are PCR positivity rates. **B)** The same type of model captures key features of observed *M. pneumoniae* dynamics 1958-1995. The fitted data are variance-stabilized numbers of samples which are simultaneously CA and MpCF-positive. (Data source: Statens Serum Institut and (2)).

the frequency  $f_0 - f_1$  corresponds to a period of 5.1 years (95%CI: [4.8, 5.5]). It should be noted that  $5\text{yr}/43.46\text{wk} = 6$  to within 1%, while 5 years is of course also an integer multiple of the period of the seasonal driver (1 year). This suggests that the system displays *subharmonic resonance* (the second mechanism for population cycling described in (43) and a well-known phenomenon in non-linear oscillatory systems (44, 45)).

Grossman remarked (42, 46) that the SIR equilibrium (w. vital dynamics) tends to be only weakly stable, since the real part of the eigenvalue (the decay rate) is much smaller than the imaginary part (the frequency). We find the same phenomenon for the SIRS system with *M. pneumoniae* parameters, with the ratio  $|\text{Im}\{\lambda\}/\text{Re}\{\lambda\}| \approx 14$  (with  $\lambda$  being the relevant eigenvalue of the Jacobian matrix for the linearized system).

A simple Fourier transform of the 2010-2020 (pre-COVID) data yields a dominant period of 5.1 years, while a Lomb-Scargle (LS) periodogram (47), which has finer frequency resolution, places the peak at 4.9 years. For the MpCF-based 1958-1995 time series, the LS periodogram shows the annual signal as being the strongest, which makes sense given the observation of (2) that the multiannual outbreak pattern was somewhat overtaken by annual dynamics during the late 1970's and early 1980's. However, the strongest multiannual peak for the whole period (1958-1995) is at 4.1yrs (LS)/4.2yrs (Fourier). If the 1958-1975 period is viewed in isolation, the strongest peak (eclipsing the annual signal as well) is at 4.6yrs (LS)/4.3yrs (Fourier). See Supplementary Fig. S2 for Fourier and LS spectra of the incidence time series.

## Demographic stochasticity

Spurred by the observation that the deterministic model will always eventually decay into annual dynamics, it is natural to ask how a departure from determinism affects the dynamics. Demographic stochasticity is a simple and ubiquitous source of noise in population dynamics (including epidemiological dynamics) (48, 49). This type of stochasticity occurs in finite populations and is fundamentally due to

1) Individuals being discrete (as opposed to the real numbers  $S$ ,  $I$  and  $R$  of a typical ordinary differential equation-based model), and

2) The presence of probability *rates* such as  $\mu$ ,  $\beta$ ,  $\gamma$  and  $\delta$ , which implies stochasticity in the timing of birth/death, infection, recovery and immune waning in finite populations.

Both of these effects can be taken into account by stochastic simulation, as may be implemented using the Doob-Gillespie algorithm (details in *Materials and Methods*) (50). With such a seasonally-forced stochastic SIRS model with vital dynamics, we find that multi-year cycles may indeed be sustained by demographic noise, suggesting that the system exhibits a stochastic resonance (42). However, clear multiannual cycles can be sustained by demographic stochasticity only in populations of less than approximately 2 million individuals, see Fig. 2. Simple demographic stochasticity alone is thus unlikely to be the source of sustained multiannual cycles in *M. pneumoniae*.

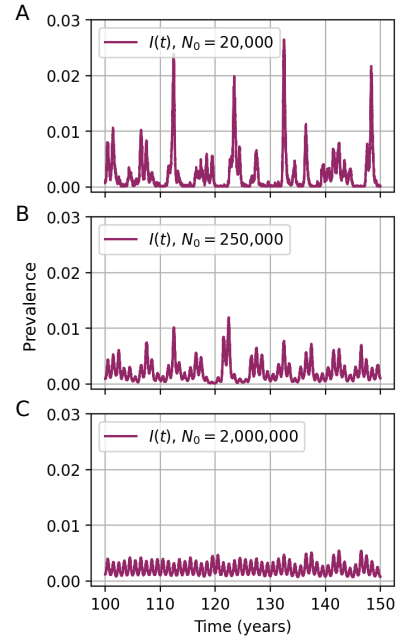


**Fig. 2. Demographic stochasticity excites multi-year cycles in smaller populations.** Doob-Gillespie simulations of a seasonally forced SIRS model parametrized with *Mycoplasma pneumoniae* parameters as determined by Bayesian fit to 2010-2025 data. **A)** In small populations (initial population size  $N_0 = 20,000$ ), demographic stochasticity leads to noisy multi-year cycles. **B)** In intermediate populations ( $N_0 = 250,000$ ), multi-year cycles are prominent and fairly regular. **C)** In larger populations ( $N_0 = 2 \times 10^6$ ), annual dynamics dominates as the impact of demographic stochasticity is smaller.

## Environmental stochasticity

We go on to consider the effects of *extra-demographic* or *environmental* stochasticity. Random fluctuations in the transmission rate  $\beta(t)$  will be the primary source of environmental stochasticity considered, but we will also explore the effects of more generic exogenous shocks to the system.

As shown in Fig. 3A, random fluctuations in the transmission rate tends to stimulate approximately 5-year cycles for a wide range of moderate noise levels. When stochasticity is very slight, the annual cycle dominates, and when environmental fluctuations are very strong, the epidemic dynamics lack predictable patterns and become dominated by large but rare outbreaks, appearing as a Fourier spectrum with all frequencies represented and no discernible peaks. Details of the implementation of stochastic transmission rates, which we base on (51), can be found in *Materials and Methods*. It should be noted that even when the annual peak is the highest, a subdominant peak with e.g. 50% of the peak power of the annual signal will lead to a prevalence timeseries that appears very clearly multiannual. The averaging process of Fig. 3A leads to broader and flatter multiannual peaks than those found in individual spectra, and for this reason Fig. 3B shows the spectra of a few individual realizations in which the peaks at approx. 5 years stand out.

While the 5-year cycle is the most typical multiannual cycle at moderate noise levels (given *M. pneumoniae* parameters), other cycles are excited as well, as shown in Fig. 3, with approximately three-year as well as 6-7 year cycles being somewhat common at moderate-to-high noise levels ( $\sigma > 0.2$ ).

In Fig. 4, we explore the immediate impact of a singular perturbation (a “kick”) to the system (52). The perturbation is implemented as either a discrete change in the infected population (Fig. 4A-C) or the susceptible population (Fig. 4D). Since only a single “kick” is given, the system will only transiently settle into a multiannual cycle and we thus measure the strength of the 5-year cycle during the 20 years immediately following the perturbation. Fig. 4A shows that the timing of the perturbation matters, with a kick during the low-transmission part of the season most likely to excite the multi-year cycle. In other words, a kick of a certain size (whether in the positive or negative direction) has a larger effect if it occurs when circulation is already low. However, Fig. 4B reveals that this seasonal dependence is completely accounted for by the *relative* magnitude of the perturbation, i.e. the change in incidence divided by the current incidence at that time. If plotted as a function of this relative magnitude,  $\Delta I/I$ , the strength of the excited cycle shows only a very faint seasonal dependence.

The annual as well as the (transient) five-year cycles are shown in the  $(S, I)$  configuration space (with  $R = 1 - S - I$  suppressed) in Fig. 4C. The rate at which  $I(t)$  and  $S(t)$  changes can be judged by the spacing between the colored markers, and the color of the markers themselves indicate the time of year. As is evident, the five-year cycle can be quite complex. The perturbation that initiated the five-year cycle is visible as the approximately vertical line connecting the annual and multiannual cycles.

## Beyond the post-COVID rebound of *M. pneumoniae*

Although the deterministic seasonal SIRS model captures the 2010-2025 dynamics well, predicting or forecasting *M.*

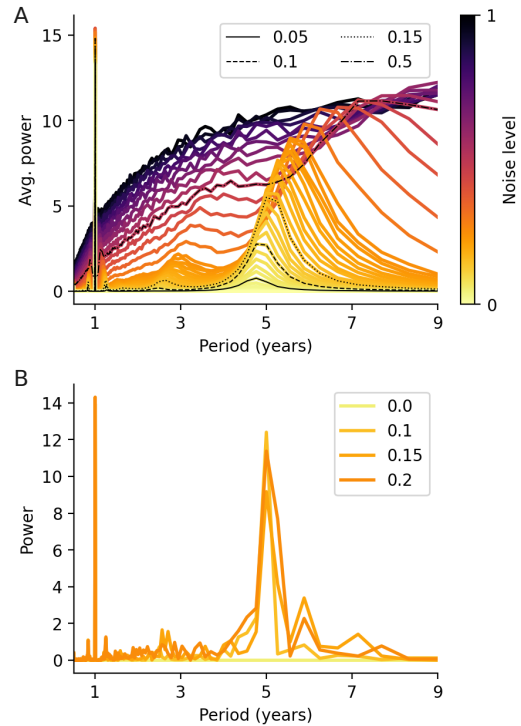


**Fig. 3. Moderate environmental noise stimulates multiannual cycles**, especially approximately 5-year cycles. **A)** Average Fourier spectrum across 1560 realizations (for each noise level indicated in the legend) of the prevalence  $I(t)$  of the seasonal SIRS model with parameters determined by a fit to 2010-2025 data from Denmark. The noise source is random fluctuations in the transmission rate  $\beta(t)$ , implemented as Gamma-distributed multiplicative noise with mean 1 and variance  $\sigma^2$  (see Methods and (51)) The *noise level* shown is the value of  $\sigma$ . Each analyzed simulation timeseries was 100 years, and a 1000 year “transient” was discarded. **B)** Fourier spectra of four individual realizations at low to moderate noise levels.

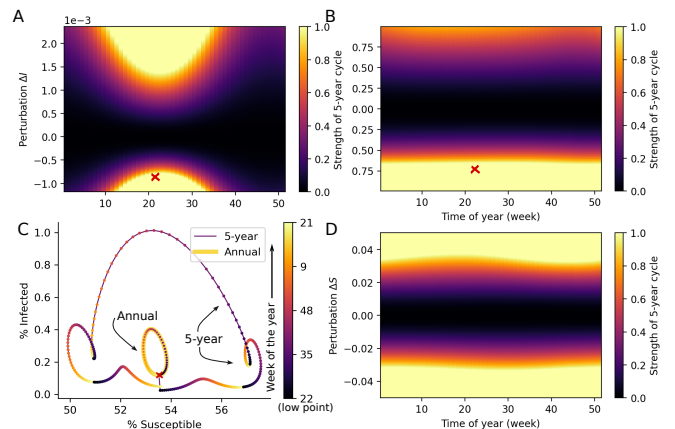


**Fig. 4. One-off exogenous perturbations (“kicks”) transiently excite multiannual cycles.** **A)** After a discrete change in prevalence of magnitude  $\Delta I$ , the system may temporarily settle into a 5-year cycle. The 5-year cycle is particularly prominent if the perturbation happens near the time of lowest prevalence. The color indicates the power of the 5-year cycle in the Fourier spectrum, relative to the highest peak. The spectrum is based on the first 20 years post-perturbation. The red cross indicates the perturbation implemented in panel D. **B)** If the magnitude of the perturbation  $\Delta I$  is proportional to the current prevalence  $I(t)$ , the prominence of the 5-year cycle ceases to depend on time of year. The red cross again indicates the perturbation implemented in panel D. **C)** Annual and 5-year cycles depicted in  $(S, I)$  configuration space. The marker color denotes the time of year, and markers are one week apart. The approximately vertical line starting from the red cross shows the exogenous “kick” which causes a transition from an annual (thick yellow line) to a 5-year cycle (thin purple line). **D)** Perturbations to  $S(t)$ , rather than the prevalence.

*pneumoniae* incidence may be challenging. We know that long-term predictions using the deterministic model are limited by its tendency to revert to annual dynamics. In the short term, however, a deterministic model may still be appropriate for forecasting. Fig. 5A shows the trajectory obtained by continuing the seasonal SIRS model for another 10 years (with parameters from the fit to 2010-2025 data). Supplementary Fig. S1 shows that the system in fact exhibits transient chaos, with a maximal local/instantaneous Lyapunov exponent (LLE) (53) that is mostly positive. A Lyapunov exponent  $\lambda$  measures sensitivity to initial conditions – which also includes the tendency of the system to amplify ( $\lambda > 0$ ) or buffer ( $\lambda < 0$ ) perturbations from e.g. noise (54). However, the arithmetic mean value of the greatest LLE during the first two years is only approx.  $10^{-3}$ /wk. In practical terms, a separation between two trajectories will have grown by only approx. 12% after the first two years of deterministic dynamics. LLEs were computed using the QR method described in (55).

Moving beyond deterministic dynamics, the effects of environmental stochasticity on predictions are shown in 5B. Here, we assume a moderately high level of environmental stochasticity ( $\sigma = 0.15$ , compare with the amplitude of seasonality at 0.19) and explore the range of predicted outcomes. The fit to empirical data is assumed known, and noise is only introduced for the prediction part of the simulations. While sensitivity to stochastic effects may complicate medium-term predictions (note the spread between realizations in 5B from 2027 onward), some short-term features are relatively robust even at this noise level. Predictions agree that 2025 is likely to be a moderate-to-high incidence year, exemplifying how deterministic models yield valuable short-term forecasts even in mildly chaotic epidemiological systems. While long-term predictions using the deterministic model are limited by its decay into annual dynamics, the presence of stochasticity limits extended prediction not only by causing variability in the incidence during any given year, but also by enabling mode-hopping, i.e. transitions between annual and multiannual cycles (49, 56), as exemplified in Supplementary Fig. S6. That the predictions for the years immediately following the large NPI-induced perturbation agree well between the stochastic and deterministic simulations fits well with the general observation that restorative forces are stronger far from equilibrium leading the stochastic model to (temporarily) behave more like the deterministic model (42).

## Limitations

In fitting the 2010-2025 time series, we used the PCR positivity rate as an incidence proxy, while we used the number of positive tests for the 1958-1995 data (total number of tests were not on record). Neither of these measures are perfect incidence proxies, and they suffer in distinct ways from biases introduced by varying testing intensities. If testing intensity is increased, this leads to an increase in the number of positive tests, while it leads to a decrease in the test positivity rate (since the denominator – the total number of tests – is increased). It may be possible to enhance fitting further by accounting for fluctuations in testing intensity when such data is available, something we have not attempted to do, beyond simple variance stabilization. Furthermore, the fidelity of the 1958-1995 data series is affected by both the (somewhat imperfect) test characteristics of the cold agglutination and

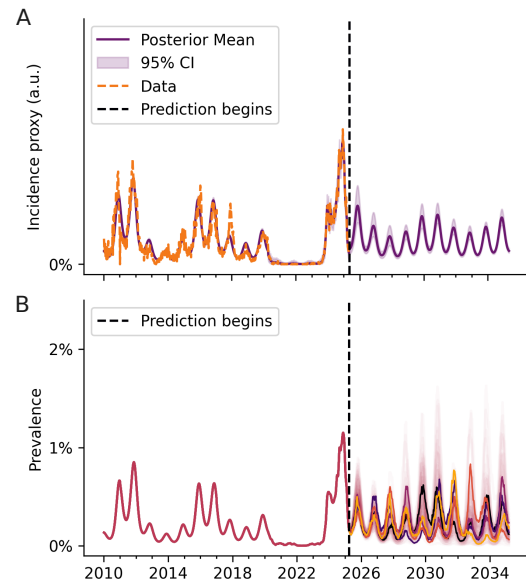


**Fig. 5. Prediction is hard.** **A)** Prediction using deterministic model, parameters fitted to 2010-2025 data. **B)** Range of predictions given identical assumptions, but including noise in transmission ( $\sigma_\beta = 0.15$ , 100 realizations). Noise can significantly affect long- and medium-term predictions, but all realizations agree that 2025 will see significant *M. pneumoniae* activity.

complement fixation tests (since the samples considered positive are those which were positive in *both* of these tests (2)). We have not taken age structure into account (57), nor have we considered spatial effects which might enhance the impact of demographic stochasticity (58).

## Discussion and conclusion

The origins of non-trivial cycles in ecological systems and the extent to which stochasticity plays a role in shaping them are long-standing questions in ecology, including epidemiology. In (59), the authors used wavelet analysis to identify 3-4 year cycles in pertussis across 12 countries and noted that the periodicity was transient in nature, in line with results of (60, 61). While the origins of the multiannual cycles of *M. pneumoniae* are generally regarded as unclear (21, 62), a few different mechanisms of varying complexity have been presented in the literature. Zhang et al. (63) suggested a combination of strain dynamics, contact network structure and waning immunity as the explanation, while Omori et al. (64) explored three different possible explanations: school-term forcing, a low-dispersion distribution of immunity duration, and interference between *M. pneumoniae* serotypes. They find that, of these three explanations, a less variable duration of immunity (compared with the typically assumed exponential waning) best captures the generally observed patterns in that it allows for incidence oscillations.

Recently, the authors of (26) used a TSIR model to describe the post-COVID rebound of *M. pneumoniae* in Denmark as well as four UN regions (Europe, Asia, the Americas, and Oceania) but found that they required at least a 90% reduction in the transmission rate due to non-pharmaceutical interventions in order to fit the data.

We find that intrinsic, noisy dynamics is sufficient to explain the complex cycles, offering a parsimonious model for

**Table 1. Estimated and assumed parameters from fit to 2010-2025 *Mycoplasma pneumoniae* surveillance data from Denmark.**

| Parameter | Description                | Estimated value [95% HPD]  |
|-----------|----------------------------|----------------------------|
| $\beta_0$ | Mean transmission rate     | 0.72/wk [0.68; 0.79]       |
| $a$       | Amplitude of seasonality   | 0.186 [0.174; 0.197]       |
| $\delta$  | Rate of waning of immunity | 1/(11.2yr) [1/14.4; 1/9.8] |
| Parameter | Description                | Assumed value              |
| $\mu$     | Birth/death rate           | 1/(80yr)                   |
| $\gamma$  | Recovery rate              | 1/(2.5wk)                  |

the dynamics of *M. pneumoniae*. Earn et al. (65) demonstrated the existence of a rich landscape of stable cycles in the seasonally driven SEIR model at high transmission rates (basic reproductive numbers in excess of approx. 4). In the current case of *M. pneumoniae* however, multiannual cycles are unstable and require stochasticity or perturbations to be sustained and appear to be a result of stochastic resonance.

With the COVID-19 NPIs phased out, another major – if less abrupt – change in *M. pneumoniae* epidemiology is on the horizon. Macrolide resistance has been growing in recent years, albeit with large geographical differences (66), and it is currently unclear how this will affect epidemiological dynamics. More generally, there is a need for comparative studies of the factors governing the diversity of complex cycles observed globally for pathogens such as *M. pneumoniae* and parvovirus B19, which may also facilitate co-estimation of environmental sources of stochasticity.

## Materials and Methods

**The seasonal SIRS model.** The seasonally-forced SIRS model with vital dynamics and constant population size is given by

$$\frac{dS}{dt} = \mu - \beta(t)S(t)I(t) + \delta R(t) - \mu S(t), \quad [1]$$

$$\frac{dI}{dt} = \beta(t)S(t)I(t) - (\gamma + \mu)I(t), \quad [2]$$

$$\frac{dR}{dt} = \gamma I(t) - (\delta + \mu)R(t), \quad [3]$$

where the instantaneous transmission rate  $\beta(t)$  is a non-negative and periodic function with a period of one year, i.e.  $\beta(t + 1\text{yr}) = \beta(t)$ . The remaining parameters are the birth/death rate  $\mu$ , recovery rate  $\gamma$  and immunity waning rate  $\delta$ . Noise in the transmission rate  $\beta(t)$  is implemented as described in (51); when numerically integrating the above set of differential equations, we draw multiplicative noise from a Gamma distribution with shape  $1/\sigma^2$  and scale  $\sigma^2$ . The parameter  $\sigma$  is the noise level referred to in Fig. 3.

**Linearization of the autonomous system.** The analogous autonomous system to equations Eq. (1)-Eq. (3) is obtained by substituting a constant transmission rate  $\beta$  in place of  $\beta(t)$  (with  $\beta$  equal to the mean of its time-varying counterpart). If released away from equilibrium,  $I(t)$  performs an underdamped oscillation before the system settles into an equilibrium configurations ( $S^*$ ,  $I^*$ ,  $R^*$ ), where:

$$S^* = \frac{\gamma + \mu}{\beta}, \quad I^* = \frac{(\beta - \mu - \gamma)(\delta + \mu)}{(\gamma + \delta + \mu)\beta}, \quad R^* = \frac{(\beta - \gamma - \mu)\gamma}{(\gamma + \delta + \mu)\beta}.$$

Linearizing the system around this equilibrium and applying a small perturbation, the decay rate and characteristic frequency are given by the eigenvalues of the Jacobian matrix:

$$J = \begin{pmatrix} \frac{\gamma\delta - \beta(\delta + \mu)}{\gamma + \delta + \mu} & -\gamma - \mu & \delta \\ \frac{(\delta + \mu)(\beta - \gamma - \mu)}{\gamma + \delta + \mu} & 0 & 0 \\ 0 & \gamma & -\delta - \mu \end{pmatrix}$$

We leave out the analytic expressions for the eigenvalues since they are exceedingly long and can be determined from the above matrix by standard methods. With the parameters fitted to the Danish 2010-2025 time series, the eigenvalues are  $\lambda_1 = -2.4 \times 10^{-4}$  and  $\lambda_{\pm} = -0.0017 \pm 0.023i$ . Since all real parts are strictly negative, the equilibrium is asymptotically stable.

**Bayesian fitting of time series.** We fit the seasonal SIRS model as described above using the probabilistic programming language Stan (67, 68), with a sinusoidal seasonally forced transmission rate  $\beta(t) = \beta_0 \xi(t)(1 + a \sin(2\pi t/\text{year} + \phi))$ , to positivity rates given in the 2010-2025 data set.  $\xi(t)$  is the NPI multiplier which is fixed to 1 until March 2020 and otherwise estimated. The priors used were:

- $\beta_0 \sim N[0; 5/T]$  where  $N[x; y]$  indicates a Gaussian (normal) distribution with mean  $x$  and standard deviation  $y$ , while  $T = 1/\gamma$  is the recovery time (2.5wk).
- NPI multipliers  $\xi(t) \sim N[0.8; 0.3]$
- $\log(\rho) \sim N[-2; 0.5]$
- $S(t=0) \sim N[0.3; 0.3]$
- $\log(x_I) \sim N[-4; 2]$  such that  $I(t=0) = x_I S(t=0)$  (the stick-breaking method, ensuring  $S(t=0) + I(t=0) \leq 1$ )
- $\phi \sim U[0; 2\pi]$  where  $U[x; y]$  indicates the uniform distribution with support on the interval  $[x, y]$
- $a \sim N[0; 0.10]$
- $\delta \sim N[1/(20\text{yr}); 1/(10\text{yr})]$
- $\rho x_{\text{data}} \sim N[x_{\text{model}}; \sigma_{\text{obs}}]$
- $\sigma_{\text{obs}} \sim N[0; 0.1]$

Here  $x_{\text{data}}$  and  $x_{\text{model}}$  refer to the measured incidence proxy (positivity rate, arbitrarily rescaled) and the modeled incidence, respectively. Note that for the parameters  $\beta_0$ ,  $\rho$ ,  $S(t=0)$ ,  $a$ ,  $\delta$ ,  $x_{\text{data}}$ ,  $\sigma_{\text{obs}}$  and the NPI multipliers, only the part of the normal distribution with positive support is used, since the parameters in question are necessarily non-negative. The fit to the 1958-1995 MpCF-based data follows similar principles and is detailed in the appendix. For the purposes of fitting, the model (Eqs. 1-3) is implemented using the efficient discretization scheme described in (25), with a time-step of 0.25wk. This discretization was used for Figs. 1, 3, 4, 5, S6, S3, S4 and S5, whereas the Lyapunov exponent calculations of Fig. S1 were performed using standard Euler integration of equations Eqs. 1-3 with a time-step of 0.05wk. Convergence was assessed based on the absence of diagnostic warnings from CmdStanPy (68), including: absence of divergent chains, no exceedances of tree-depth, sufficient E-BFMI ( $> 0.3$ ), and satisfactory  $\hat{R}$  ( $< 1.05$ ) and effective sample size (bulk ESS  $> 100 \times \#\text{chains}$ ) for all parameters.

**Doob-Gillespie simulations.** The stochastic simulations of Fig. 2 are based on the following system of transition rates:

$$\begin{aligned} r[\emptyset \rightarrow S] &= \mu N, \\ r[S \rightarrow \emptyset] &= \mu S, \\ r[I \rightarrow \emptyset] &= \mu I, \\ r[R \rightarrow \emptyset] &= \mu R, \\ r[S \rightarrow I] &= \begin{cases} \beta(t)SI/N & \text{if } N > 0, \\ 0 & \text{otherwise,} \end{cases} \\ r[I \rightarrow R] &= \gamma I, \\ r[R \rightarrow S] &= \delta R, \end{aligned} \quad [4]$$

with the time-dependent transmission rate given by  $\beta(t) = \beta_0(1 + a \sin(2\pi t/\text{year} + \phi))$ . Denoting the above rates by  $r_i$ ,  $i \in \{1, \dots, 7\}$ , the Doob-Gillespie algorithm (50) thus prescribes iteratively propagating the state of the system by drawing a uniformly distributed random number  $r_1 \in [0, 1]$ , determining the time to next event  $\tau = -(\sum_i r_i)^{-1} \log(r_1)$  and the nature of the event by drawing another random uniform number  $r_2 \in [0, 1]$  and determining the smallest  $j$  for which  $\sum_{i=1}^j r_i > r_2 \sum_{i=1}^7 r_i$ . Event (or “reaction”)  $j$  is then performed and the time is incremented by  $\tau$ . The procedure is then reiterated until the desired final time is reached.

**ACKNOWLEDGMENTS.** We thank the Statens Serum Institut (SSI) for providing Danish surveillance data. BFN acknowledges financial support from the Carlsberg Foundation (grant no. CF23-0173). SWP is a Peter and Carmen Lucia Buck Foundation Awardee of the Life Sciences Research Foundation. MHJ is supported by the Novo Nordisk Foundation, grants NNF20OC0064978 and NNF24OC0089788. BTG would like to acknowledge support from Princeton Catalysis and Princeton Precision Health.

1. RL Kradin, *Understanding Pulmonary Pathology: Applying Pathological Findings in Therapeutic Decision Making*. (Academic Press), pp. 157–244 (2016).
2. K Lind, M Benzon, S Jensen, W Clyde, A seroepidemiological study of mycoplasma pneumoniae infections in denmark over the 50-year period 1946–1995. *Eur. J. Epidemiol.* **13**, 581–586 (1997).
3. HM Foy, *Mycoplasma pneumoniae*, eds. AS Evans, HA Feldman. (Springer US, Boston, MA), pp. 345–366 (1982).
4. HM Foy, Infections caused by mycoplasma pneumoniae and possible carrier state in different populations of patients. *Clin. Infect. Dis.* **17**, S37–S46 (1993).
5. GS Braun, KS Wagner, BD Huttner, H Schmid, *Mycoplasma pneumoniae*: usual suspect and unsecured diagnosis in the acute setting. *The J. emergency medicine* **30**, 371–375 (2006).
6. M Narita, Pathogenesis of extrapulmonary manifestations of mycoplasma pneumoniae infection with special reference to pneumonia. *J. infection chemotherapy* **16**, 162–169 (2010).
7. S Kumar, Mycoplasma pneumoniae: A significant but underrated pathogen in paediatric community-acquired lower respiratory tract infections. *Indian J. Med. Res.* **147**, 23–31 (2018).
8. S Martinez-Cabrales, et al., Preliminary summary and reclassification of cases from the pediatric research of management in stevens-johnson syndrome and epidermolysis (promise) study: A north american, multisite retrospective cohort. *J. Am. Acad. Dermatol.* **90**, 635–637 (2024).
9. TN Canavan, EF Mathes, I Frieden, K Shinkai, Mycoplasma pneumoniae-induced rash and mucositis as a syndrome distinct from stevens-johnson syndrome and erythema multiforme: a systematic review. *J. Am. Acad. Dermatol.* **72**, 239–245 (2015).
10. J Hasbini, N Safawi, C Berjaoui, M Rajab, A Naous, Mycoplasma pneumoniae complicated by stevens-johnson syndrome: A case report. *Respir. Medicine Case Reports* **51**, 102081 (2024).
11. KA Ravin, et al., Mycoplasma pneumoniae and atypical stevens-johnson syndrome: a case series. *Pediatrics* **119**, e1002–e1005 (2007).
12. F Sánchez-Vargas, O Gómez-Duarte, Mycoplasma pneumoniae—an emerging extrapulmonary pathogen. *Clin. microbiology infection* **14**, 105–115 (2008).
13. M Asif, et al., Heart failure associated with mycoplasma pneumoniae infection, a case and review of literature. *J. Community Hosp. Intern. Medicine Perspectives* **13**, 55 (2023).
14. GH Cassell, BC Cole, Mycoplasmas as agents of human disease. *New Engl. J. Medicine* **304**, 80–89 (1981).
15. KB Waites, DF Talkington, Mycoplasma pneumoniae and its role as a human pathogen. *Clin. microbiology reviews* **17**, 697–728 (2004).
16. B Bajantri, S Venkatram, G Diaz-Fuentes, Mycoplasma pneumoniae: a potentially severe infection. *J. clinical medicine research* **10**, 535 (2018).
17. JW Kim, et al., Mycoplasma pneumoniae pneumonia in korean children, from 1979 to 2006-a meta-analysis. *Clin. Exp. Pediatr.* **52**, 315–323 (2009).
18. RJ Brown, et al., Mycoplasma pneumoniae epidemiology in england and wales: a national perspective. *Front. microbiology* **7**, 157 (2016).
19. Y Wang, et al., Epidemiological characteristics of mycoplasma pneumoniae respiratory tract infection in hospitalized children from 2006 to 2013. *Int J Clin Exp Pathol* **10**, 5955–5963 (2017).
20. W Rastawicki, S Kaluzewski, M Jagielski, R Gierczynski, Epidemiology of mycoplasma pneumoniae infections in poland: 28 years of surveillance in warsaw 1970-1997. *Euro surveillance: bulletin Eur. sur les maladies transmissibles= Eur. communicable disease bulletin* **3**, 99–100 (1998).
21. V Chalker, T Stocki, M Mentasti, D Fleming, T Harrison, Increased incidence of mycoplasma pneumoniae infection in england and wales in 2010: multocus variable number tandem repeat analysis typing and macrolide susceptibility. *Eurosurveillance* **16**, 19865 (2011).
22. BT Grenfell, ON Bjørnstad, J Kappey, Travelling waves and spatial hierarchies in measles epidemics. *Nature* **414**, 716–723 (2001).
23. G Rozhnova, CJE Metcalf, BT Grenfell, Characterizing the dynamics of rubella relative to measles: the role of stochasticity. *J. The Royal Soc. Interface* **10**, 20130643 (2013).
24. MJ Keeling, P Rohani, BT Grenfell, Seasonally forced disease dynamics explored as switching between attractors. *Phys. D: Nonlinear Phenom.* **148**, 317–335 (2001).
25. SW Park, et al., Predicting the impact of non-pharmaceutical interventions against covid-19 on mycoplasma pneumoniae in the united states. *Epidemics* **49**, 100808 (2024).
26. PMM Sauter, et al., Global spatiotemporal dynamics of mycoplasma pneumoniae re-emergence after covid-19 pandemic restrictions: an epidemiological and transmission modelling study. *The Lancet Microbe* (2025).
27. EJ Chow, TM Uyeke, HY Chu, The effects of the covid-19 pandemic on community respiratory virus activity. *Nat. Rev. Microbiol.* **21**, 195–210 (2023).
28. M Koutsakos, AK Wheatley, K Laurie, SJ Kent, S Rockman, Influenza lineage extinction during the covid-19 pandemic? *Nat. Rev. Microbiol.* **19**, 741–742 (2021).
29. S Caini, et al., Probable extinction of influenza b/yamagata and its public health implications: a systematic literature review and assessment of global surveillance databases. *The Lancet Microbe* (2024).
30. PMM Sauter, et al., Mycoplasma pneumoniae: delayed re-emergence after covid-19 pandemic restrictions. *The Lancet Microbe* **5**, e100–e101 (2024).
31. BL Boyanton Jr, RA Frenner, A Ingold, L Ambroggio, JL Kennedy, Sars-cov-2 pandemic non-pharmacologic interventions temporally associated with reduced pediatric infections due to mycoplasma pneumoniae and co-infecting respiratory viruses in arkansas. *Microbiol. Spectr.* **12**, e02908–23 (2024).
32. BG Fischer, A Baduashvili, AT Evans, Cold agglutinins in mycoplasma infection. *JAMA* **320**, 1038–1039 (2018).
33. JT Grayston, et al., Mycoplasma pneumoniae infections: clinical and epidemiologic studies. *JAMA* **191**, 369–374 (1965).
34. MF Beersma, et al., Evaluation of 12 commercial tests and the complement fixation test for mycoplasma pneumoniae-specific immunoglobulin g (igg) and igm antibodies, with pcr used as the “gold standard”. *J. Clin. Microbiol.* **43**, 2277–2285 (2005).
35. HM Foy, GE Kenny, MK Cooney, ID Allan, G van Belle, Naturally acquired immunity to pneumonia due to mycoplasma pneumoniae. *J. Infect. Dis.* **147**, 967–973 (1983).
36. S Zhao, SS Musa, J Qin, D He, Phase-shifting of the transmissibility of macrolide-sensitive and resistant mycoplasma pneumoniae epidemics in hong kong, from 2015 to 2018. *Int. J. Infect. Dis.* **81**, 251–253 (2019).
37. A Russcher, et al., Changing epidemiology of parvovirus b19 in the netherlands since 1990, including its re-emergence after the covid-19 pandemic. *Sci. Reports* **14**, 9630 (2024).
38. N Nicolay, S Cotter, Clinical and epidemiological aspects of parvovirus b19 infections in ireland, january 1996-june 2008. *Eurosurveillance* **14**, 19249 (2009).
39. A Bosman, J Wallinga, A Kroes, Fifth disease every four years: parvovirus b19. *Infectieziektenbulletin* **6**, 215–219 (2002).
40. M Enders, A Weidner, G Enders, Current epidemiological aspects of human parvovirus b19 infection during pregnancy and childhood in the western part of germany. *Epidemiol. & Infect.* **135**, 563–569 (2007).
41. AJ Vyse, NJ Andrews, LM Hesketh, R Pebody, The burden of parvovirus b19 infection in women of childbearing age in england and wales. *Epidemiol. & Infect.* **135**, 1354–1362 (2007).
42. MJ Keeling, P Rohani, *Modeling infectious diseases in humans and animals*. (Princeton university press), (2008).
43. R Nisbet, W Gurney, A simple mechanism for population cycles. *Nature* **263**, 319–320 (1976).
44. RM Nisbet, WS Gurney, Population dynamics in a periodically varying environment. *J. Theor. Biol.* **56**, 459–475 (1976).
45. J Guckenheimer, P Holmes, *Nonlinear oscillations, dynamical systems, and bifurcations of vector fields*. (Springer Science & Business Media) Vol. 42, (2013).
46. Z Grossman, Oscillatory phenomena in a model of infectious diseases. *Theor. population biology* **18**, 204–243 (1980).
47. TP Robitaille, et al., Astropy: A community python package for astronomy. *Astron. & Astrophys.* **558**, A33 (2013).
48. S Engen, Ø Bakke, A Islam, Demographic and environmental stochasticity-concepts and definitions. *Biometrics* pp. 840–846 (1998).
49. BT Grenfell, ON Bjørnstad, BF Finkenstädt, Dynamics of measles epidemics: scaling noise, determinism, and predictability with the tsir model. *Ecol. monographs* **72**, 185–202 (2002).
50. DT Gillespie, Exact stochastic simulation of coupled chemical reactions. *J. Phys. Chem.* **81**, 2340–2361 (1977).
51. D He, EL Ionides, AA King, Plug-and-play inference for disease dynamics: measles in large and small populations as a case study. *J. Royal Soc. Interface* **7**, 271–283 (2010).
52. P Rohani, MJ Keeling, BT Grenfell, The interplay between determinism and stochasticity in childhood diseases. *The Am. Nat.* **159**, 469–481 (2002).
53. M Jensen, G Paladin, A Vulpiani, Intermittency in a cascade model for three-dimensional turbulence. *Phys. Rev. A* **43**, 798 (1991).
54. M Pascual, P Mazzega, Quasicycles revisited: apparent sensitivity to initial conditions. *Theor. Popul. Biol.* **64**, 385–395 (2003).
55. T Okushima, Finite-time lyapunov exponents in many-dimensional dynamical systems. *Geom. Struct. Phase Space Multidimens. Chaos: Appl. to Chem. React. Dyn. Complex Syst.* **130**, 501–518 (2005).
56. M Hellberg, RA Kellogg, S Krishna, S Tay, MH Jensen, Noise induces hopping between  $nf-kb$  entrainment modes. *Cell systems* **3**, 532–539 (2016).
57. AC Nordholm, et al., Mycoplasma pneumoniae epidemic in denmark, october to december, 2023. *Eurosurveillance* **29**, 2300707 (2024).
58. O Ovaskainen, SJ Cornell, Space and stochasticity in population dynamics. *Proc. Natl. Acad. Sci.* **103**, 12781–12786 (2006).
59. H Broutin, JF Guégan, E Elguero, F Simondon, B Cazelles, Large-scale comparative analysis of pertussis population dynamics: periodicity, synchrony, and impact of vaccination. *Am. journal epidemiology* **161**, 1159–1167 (2005).
60. P Rohani, DJ Earn, BT Grenfell, Opposite patterns of synchrony in sympatric disease metapopulations. *Science* **286**, 968–971 (1999).
61. CJE Metcalf, ON Bjørnstad, BT Grenfell, V Andreasen, Seasonality and comparative dynamics of six childhood infections in pre-vaccination copenhagen. *Proc. Royal Soc. B: Biol. Sci.* **276**, 4111–4118 (2009).
62. M Xu, et al., Molecular epidemiology of mycoplasma pneumoniae pneumonia in children, wuhan, 2020–2022. *BMC microbiology* **24**, 23 (2024).
63. XS Zhang, H Zhao, E Vynnycky, V Chalker, Positively interacting strains that co-circulate within a network structured population induce cycling epidemics of mycoplasma pneumoniae. *Sci. reports* **9**, 541 (2019).
64. R Omori, Y Nakata, HL Tessmer, S Suzuki, K Shibayama, The determinant of periodicity in mycoplasma pneumoniae incidence: an insight from mathematical modelling. *Sci. reports* **5**, 14473 (2015).
65. DJ Earn, P Rohani, BM Bolker, BT Grenfell, A simple model for complex dynamical transitions in epidemics. *science* **287**, 667–670 (2000).
66. K Kim, et al., Global trends in the proportion of macrolide-resistant mycoplasma pneumoniae infections: a systematic review and meta-analysis. *JAMA network open* **5**, e2220949–e2220949 (2022).
67. Stan Development Team, Stan reference manual (2024) v2.36.0, <https://mc-stan.org>.
68. Stan Development Team, CmdStanPy (2024) v1.2.5, <https://pypi.org/project/cmdstanpy>.

## SI Appendix

**Quantifying chaos: Lyapunov exponents** In Fig. S1A, the instantaneous Lyapunov exponents  $\lambda_i(t)$  of the system are given. In Fig. S1B, we present the mean Lyapunov exponents during the first  $T$  years, i.e.  $\frac{1}{T} \int_0^T \lambda(t) dt$ . Local Lyapunov exponents were computed using the QR method described in (55).

**Bayesian fitting of 1958-1995 MpCF data** As for the 2010-2025 data, we fit a seasonal SIRS model using the probabilistic programming language Stan (67, 68), with a sinusoidal seasonally forced transmission rate  $\beta(t) = \beta_0(1 + a \sin(2\pi t/\text{year} + \phi))$ . We fit the modeled incidence to the variance-stabilized (square root-transformed) number of samples simultaneously positive for CA and MpCF (test data from (2)). There are no NPI multipliers in this fit, but to account for slowly changing contact rates and ascertainment patterns over the years, we included multipliers for the transmission rate  $\beta(t)$  and the  $\rho$ , the constant of proportionality between measured and simulated incidence. These multipliers had relatively narrow priors centered around unity and were piecewise constant for each four years of the simulation. The priors used for the 1958-1995 fit were mostly similar to those for the 2010-2025 fit, but due to the superior data quality of the 2010-2025 data, we constrained some variables using results from that fit:

- $\beta_0 \sim N[0; 5/T]$  where  $N[x; y]$  indicates a Gaussian (normal) distribution with mean  $x$  and standard deviation  $y$ . However, the variable  $\beta_0$  was itself constrained to the interval  $[1.3/T; 2.2/T]$ .
- $\log(\rho) \sim N[-2; 0.5]$
- $S(t=0) \sim N[0.3; 0.3]$
- $\log(x_I) \sim N[-4; 2]$  such that  $I(t=0) = x_I S(t=0)$  (the stick-breaking method, ensuring  $S(t=0) + I(t=0) \leq 1$ )
- $\phi \sim U[0; 2\pi]$  where  $U[x; y]$  indicates the uniform distribution with support on the interval  $[x, y]$
- $a \sim N[0; 0.10]$
- $\beta(t)$  multipliers  $\sim N[1; 0.05]$
- $\rho$  multipliers  $\sim N[1; 0.2]$
- $\rho x_{\text{data}} = N[x_{\text{model}}; \sigma_{\text{obs}}]$
- $\sigma_{\text{obs}} \sim N[0; 0.01]$

Here  $x_{\text{data}}$  and  $x_{\text{model}}$  refer to the measured incidence proxy and the modeled incidence, respectively.  $\rho$  is a constant of proportionality between the two. Note that for the parameters  $\beta_0$ ,  $\rho$ ,  $S(t=0)$ ,  $a$ ,  $x_{\text{data}}$ ,  $\sigma_{\text{obs}}$  and the  $\beta(t)$  and  $\rho$  multipliers, only the part of the normal distribution with positive support is used, since the parameters in question are necessarily non-negative. The immunity rate of waning  $\delta$  was fixed at the value obtained in the 2010-2025 plot.

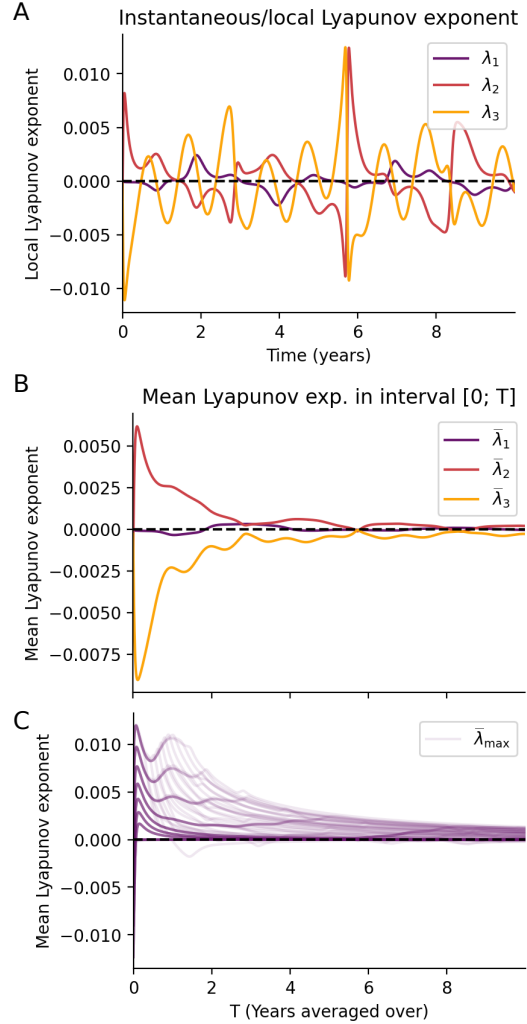


**Fig. S1. Lyapunov exponents show transient chaos** **A)** Local Lyapunov exponents  $\lambda_i(t)$ . The initial condition (at  $t = 0$ ) corresponds to the initial state (January 2010) of the 2010-2025 fit. **B)** Cumulative mean local Lyapunov exponents during the first  $T$  years, i.e.  $\frac{1}{T} \int_0^T \lambda(t) dt$ . **C)** Same as panel B, but for a wide range of initial conditions, and only the largest Lyapunov exponent is shown.

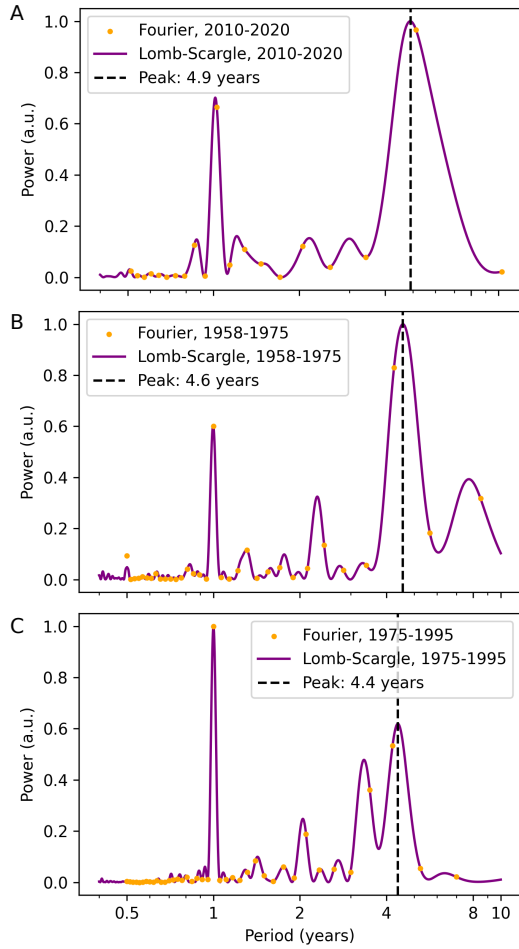


**Fig. S2. Fourier spectra and Lomb-Scargle periodograms for Danish *M. pneumoniae* incidence time series.** **A)** Spectra for the period January 2010 - March 2020 (prior to COVID-19 public health interventions). **B)** Spectra for the period February 1958 - January 1975. **C)** Spectra for the period January 1975 - November 1995.

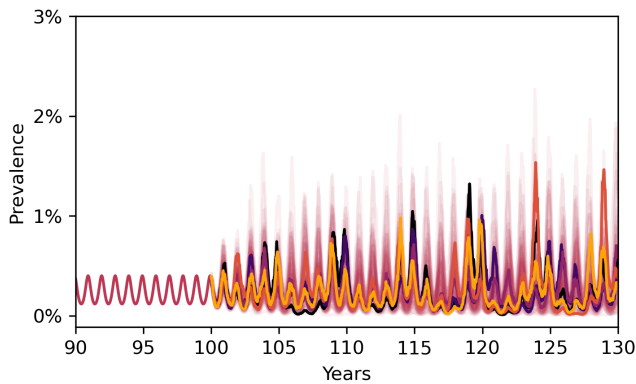


**Fig. S3. Noise in transmission excites multiannual cycles starting from the annual attractor.** After allowing the system to settle on the annual attractor, noise in the transmission rate  $\beta(t)$  is "turned on" (noise level  $\sigma = 0.15$ ) at  $t = 100$ yr. 100 realizations are shown, with five of them highlighted to clearly show the multiannual cycles which develop.

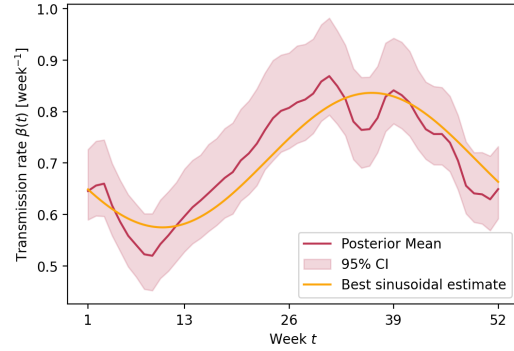


**Fig. S4. Seasonally varying transmission rate.** The dark red curve is the transmission rate obtained when fitting a seasonal profile. The orange curve is the transmission rate when instead imposing that  $\beta(t) = \beta_0(1 + a \sin(2\pi t/\text{year} + \phi))$  and fitting the parameters  $\beta_0$ ,  $a$ , and  $\phi$ .

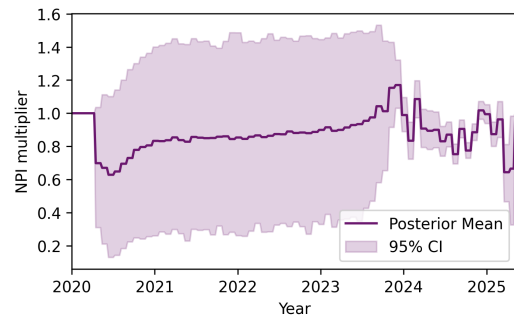


**Fig. S5. NPI multipliers.** Estimated transmission rate modulating factor. Until March 2020, this multiplier was fixed at 1.0.

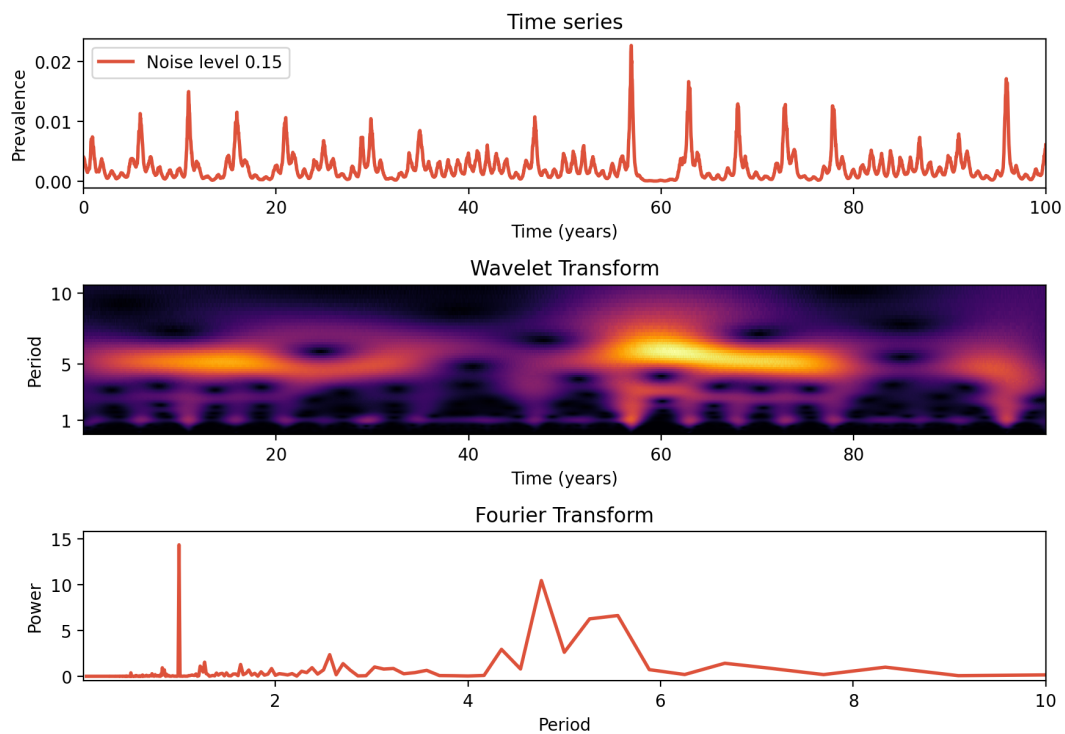


**Fig. S6. The seasonal SIRS model with (environmental) noise exhibits mode-hopping. A)** 100-year simulated time-series with noise level  $\sigma = 0.15$ . **B)** Continuous wavelet transform of the signal from panel A. **C)** Fourier transform of the entire 100-year time series. The wavelet transform confirms that the system transitions in and out of an approximately 5-year cycle, sometimes displaying primarily annual dynamics.